# Uncertainty Quantification of Thickness Estimation Via Full-Field Ultrasonic Inspection

NEEL SHAH[1], ERICA M. JACOBSON[1], ERIC B. FLYNN[2] and ADAM J. WACHTOR[1]

**ABSTRACT**

Acoustic steady-state excitation spatial spectroscopy (ASSESS) is a full-field ultrasonic inspection technique that can be utilized for structural health monitoring applications. ASSESS can rapidly identify damage or defects over a 360° field of view of a structure using geometry mapping and a scanning laser Doppler vibrometer (LDV) – enabling inspection and characterization across multiple large surfaces in a single measurement. However, variables like the incidence angle between the surface and LDV beam change when inspecting large or geometrically complex structures; greatly affecting the signal-to-noise ratio (SNR) of the measurement and the accuracy of damage estimation to an extent that has not previously been quantified.

This work experimentally quantifies the uncertainty of thickness estimation derived from full-field steady-state wave fields over various incidence angles to provide trusted operating bounds. A rotation stage and hexapod assembly were used to orient an aluminum plate with manufactured thickness losses to up to 80° both horizontally and vertically in increments of 5°. The plate specimen was designed with an assortment of manufactured damage, including discrete regions with both continuous and discontinuous material thickness loss. An affixed transducer excited the plate with a 199 kHz tone and an LDV recorded local surface response velocities. A LiDAR was used to measure the inspection surface geometry and random sample consensus (RANSAC) planar extraction was utilized to determine the orientation of the specimen with respect to the LDV and correct perspective distortions in the wavefield.

This work lays an essential foundation for identifying physical limitations of the measurement system for scanning large and complex structures and providing quantified uncertainties for detected damage within a trusted operating range – an imperative step for adoption of this inspection technique within highly standardized industries.

[1]Engineering Institute, Los Alamos National Laboratory, Los Alamos, NM 87545
[2]Space Remote Sensing and Data Science, Los Alamos National Laboratory, Los Alamos, NM 87545

## INTRODUCTION

Ultrasonic nondestructive evaluation (NDE) has a promising application for structural health monitoring (SHM) as a non-contact method with a large field of vision (FOV) [1]. However, an unquantified physical limitation exists as less light is reflected to the sensor as the incidence angle between the laser Doppler vibrometer (LDV) and the inspected surface increase while scanning large convex or planar structures. Many SHM interests involve convex geometries, like boat hulls or airplane fuselages [2], thus it is necessary to quantify how uncertainty changes with the increase of incidence angle to provide a trusted operating range, maximizing the scan range while maintaining measurement reliability.

Acoustic steady-state excitation spatial spectroscopy (ASSESS) is a technology that can identify defects over a 360-degree FOV orders of magnitude faster than typical ultrasound NDE techniques, making it especially practical for scanning large structure [3]. ASSESS achieves this by exciting structures with a continuous harmonic steady-state ultrasonic tone via a piezoelectric transducer and measuring the structure's steady state surface velocity response within the 360-degree FOV using a custom scanning LDV [4]. A LiDAR simultaneously collects geometry information to correct for perspective distortions within plate-like surface responses using post processing algorithms [5]. Local wavenumber is estimated from this corrected surface velocity response through a succession of 2D band pass spatial filters [6]. The local wavenumber estimation is smoothed in post processing and is then used to highlight various defects within a structure, including material loss, corrosion, delamination, and porosity [7][8]. The measurement resolution is defined by the chosen angular pitch of the LDV's local spherical coordinate system, which increases the effective step size over a convex structure when scanning away from a perpendicular scan region as illustrated in Figure 1. This is another uncharacterized source of uncertainty as incidence angles increase. The insight gained from this work aides in identifying the effective operating FOV and hardware/software limits of scanning ultrasonic NDE techniques comparable to ASSESS for a range of defect severities, types, and sizes.

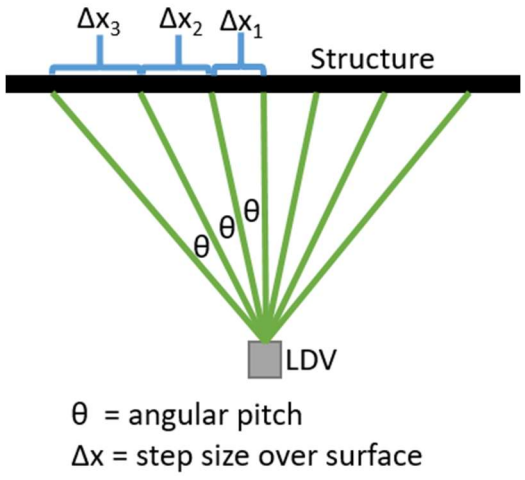


Figure 1. Illustration of effective step size increasing over scan area.

## METHODS

The test sample was a 10 mm thick bead-blasted 6061 aluminum plate with numerous built-in defects with thickness reductions ranging from 0 mm (no defect) to 9 mm (severe thinning including: a linear gradient ramp, a 12 step ramp, and 8 bores (one bore and step represent the nominal 10 mm plate thickness). Features are at least one feature size (a bore diameter) from one another and plate edges to limit effects of acoustic wave interactions with defect and plate edges.

Features are sectioned into 8 groups representing different thickness ranges for comparison [Fig 1]. The bores were designed to determine thickness estimation uncertainty for discontinuous defects. The step ramp was designed to evaluate uncertainties distinguishing different thicknesses within a large region with discontinuous defects, such as accidental cuts or gouges incurred in manufacturing environments. Lastly, the gradient ramp enables evaluation of uncertainties distinguishing thickness gradients with gradual thickness changes like that which can occur with corrosion/delamination. The opposing ramps also make it difficult to over fit processing parameters to this specific test plate, making for a more generalizable study. Any post-processing techniques of the wavenumber estimate, e.g. median-filter smoothing, that benefit from localizing the gradient feature, hinder the localization of the step feature, and vice versa. Processing parameters were heuristically chosen to balance thickness accuracy, localization, and consistency across all features in the zero-rotation orientation. A ground truth map was created from the manufacturing inspection report (Figure 2).

The sample was mounted 2.24 m away from the ASSESS system. The specimen is rotated using a rotation stage (Thorlabs HDR50), a hexapod (Physical Instrument H-811.S2), and a series of mounting adapters to test incidence angles up to 80° both horizontally and vertically, in 5° increments (Figure 3).

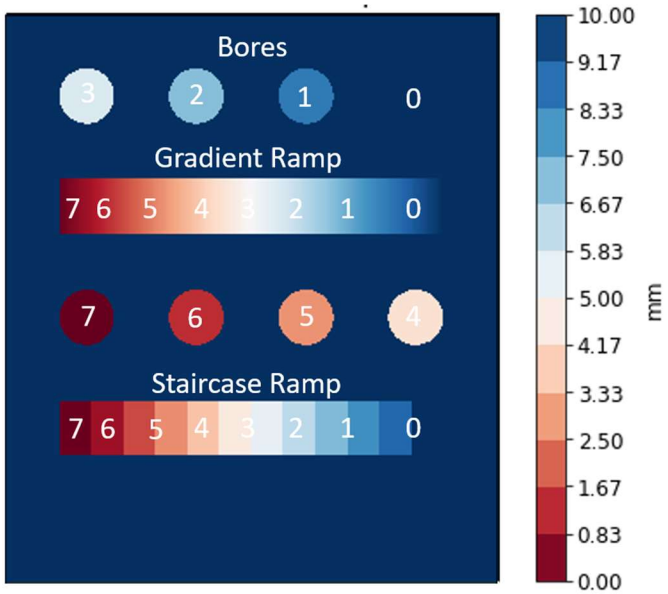


Figure 2. Ground truth thickness map for test specimen with the thickness values displayed on the color bar, and the group number displayed on the specimen geometry.

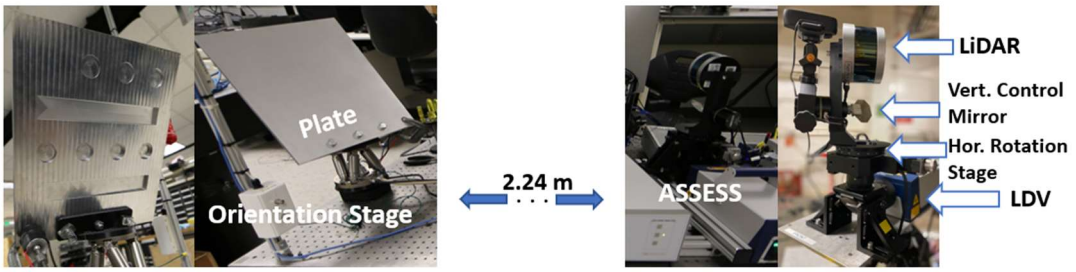

Figure 3. Experimental setup showing the ASSESS system and test plate hardware.

The system excites the plate through a clamped transducer driven at 199 kHz produced by a data acquisition system (NI USB-6363). The LDV (Polytec Vibroflex QTec) beam was rastered across the plate using a rotation stage (Thorlabs HDR50) and a galvanometer mirror for horizontal and vertical control. The LiDAR unit (Velodyne Puck Hi-Res) simultaneously collected a point cloud of the scan region geometry. The coordinate systems of the LDV measurements and LiDAR were manually registered together.

Two scans were taken at each incidence angle tested: angular pitch was kept constant during the first and adjusted for the second proportional to the reduced perceived area. The angular pitch determines the number of samples collected at each "pixel," and was proportionally changed to compensate for the effect of perspective between the plate and LDV. These two measurement sets provided a means for determining the effect of using a constant pixel pitch in real-world measurements for which large incidence angles would be present. The constant angular pitch of .015° x .015° was chosen to prevent spatial aliasing resolving the smallest theoretical wavelength corresponding to 1 mm thick sections of the plate at the most severe angles tested, therefore attributing any difference between these two scans to hardware/processing limits at severe angles.

For each scan, the collected point cloud was cropped to the plate and RANSAC planar extraction was used to extract the resulting normal with respect to the LDV, i.e. incidence angle, and the perspective was corrected accordingly as described in [5] to eliminate perspective distortions. The local wavenumber is mapped to thickness using the material's dispersion curves as described in [6]. Thickness estimates were registered to the ground truth map using translation/rotation transformations and manually selected key points from the centers of identified bores and the severe edge of ramps within the thickness estimate map using OpenCV [9]. Thickness estimates for incidence angles where no features for registration were discernible were excluded from the final dataset.

## STATISTICAL METHODS

Residual distributions were calculated through a pixel-wise subtraction of the registered thickness estimate and ground truth map. This was performed for each thickness group and only the nominal defect regions to evaluate thickness estimation uncertainty. Due to poor localization in severe angle cases (see Figure 3 for an example), the residuals were masked to isolate thickness estimation uncertainty from localization ability. The resulting residual distributions were well sampled ($n > 500$), treated as Gaussian, and the median and 95% confidence intervals were recorded. Another

distribution was created in which the ramp groups were expanded horizontally by 10 mm to determine inter-defect thickness separation and uncertainty.

Residuals were not assumed to be centered on zero to not account for under/over estimation. By default, the center is determined by using the mode of the binned residual distribution if it falls between +/- 2.5 mm. In severe angle cases where the mode may fall outside of that range, two normal distributions made up the residual distribution: one smaller curve representing the poorly localized thickness estimate, and another representing where the spatial-based processing was largely unable to accurately estimate the nominal plate thickness. The first is masked for by enforcing two groups using k-means clustering using Scikit-Learn and using the center of the cluster closest to zero as the center of the distribution [10]. If the absolute value of the residual center was greater than 3 mm, it was considered to be outside the viable analysis range and subsequently not included in the final dataset. Group 1 required a more stringent threshold for its mode to fall within +- 1 mm before relying on k-means clustering to mask for the estimation.

## RESULTS & DISCUSSION

For brevity, results for three thickness groups are reported in this paper. Group 0 and Group 7 represent the bounding thickness cases for the test plate and Group 2 provides another reference for performance at higher thickness where there is less sensitivity in the thickness estimation because of the flatness of the dispersion curves in that range.

Three types of defect features were chosen to successfully reveal different performance characteristics within each thickness group. The bores behaved as small individual defects with distinct edges. The stepped ramp behaved as one large defect with numerous edge boundaries that provided ample opportunities for reflections and pooling of the acoustic waves, and thus was more easily resolved by ASSESS. The gradient ramp behaves as one large defect as well. However, because of the continuous geometry of this defect, the acoustic waves were able to more easily escape, and thus provided an operating range between the other two features. The normal assumption for the residual distributions was found to hold for most groups. Group 0 behaved like the left half of a normal distribution as the processing parameters used for ASSESS rarely overestimated past the nominal thickness of the plate.

For the following figures, *rMu* refers to the residual distribution median, *rLb* to the lower bound of the 95% confidence interval, and *rUb* to the upper bound. The left summarizes the constant pitch measurements, while the right summarizes the compensated pitch measurements. Each column refers to a defect, and each row displays the results of each feature. Each tile within each subplot shows the residuals of the estimated thickness (in mm). A red color indicates underestimation, while a blue color indicates overestimation. Black tiles are measurements that fall outside of the viable analysis range.

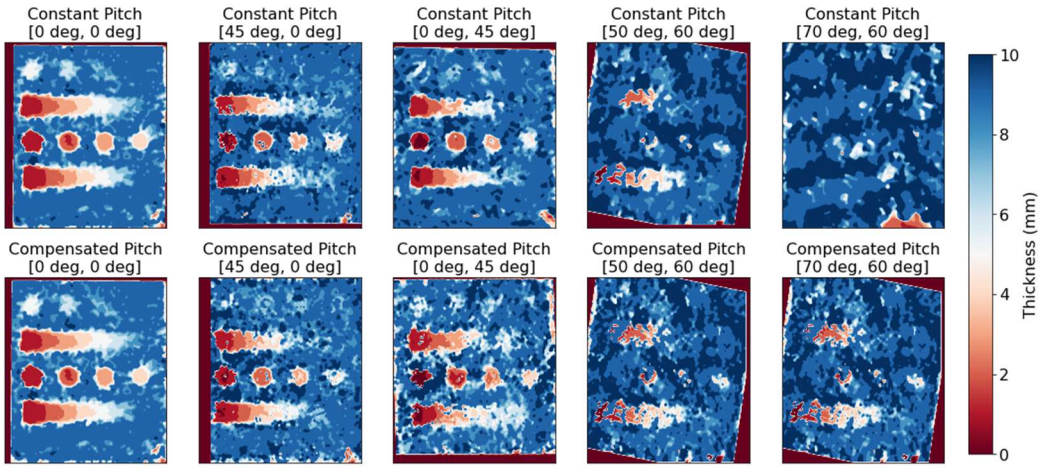


Figure 4. Measurements at various incidence angles – note how the largest incidence angle measurements have limited discernable features.

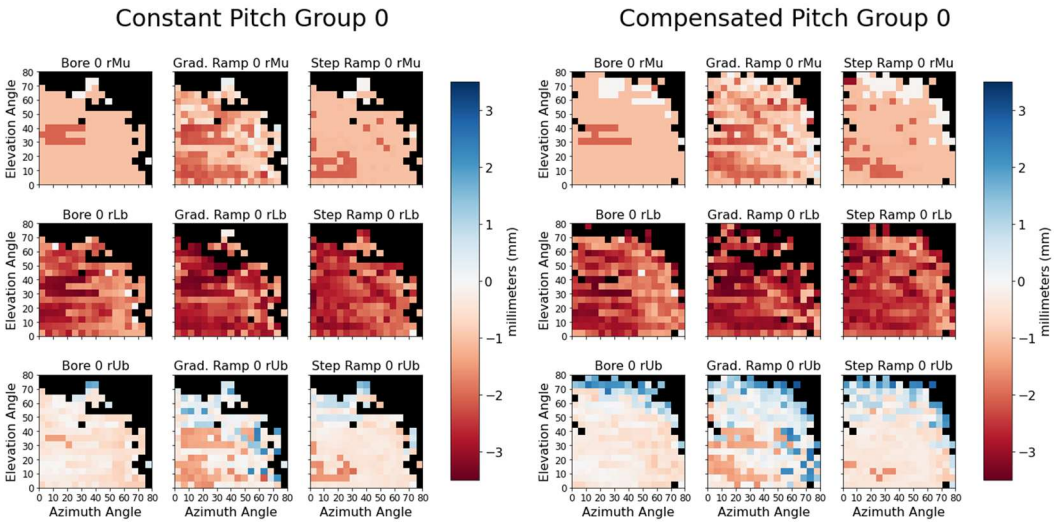


Figure 5. Residual statistics for thickness group zero (absolute thickness of 9.72 – 10 mm, or a thickness reduction of 0% – 3%).

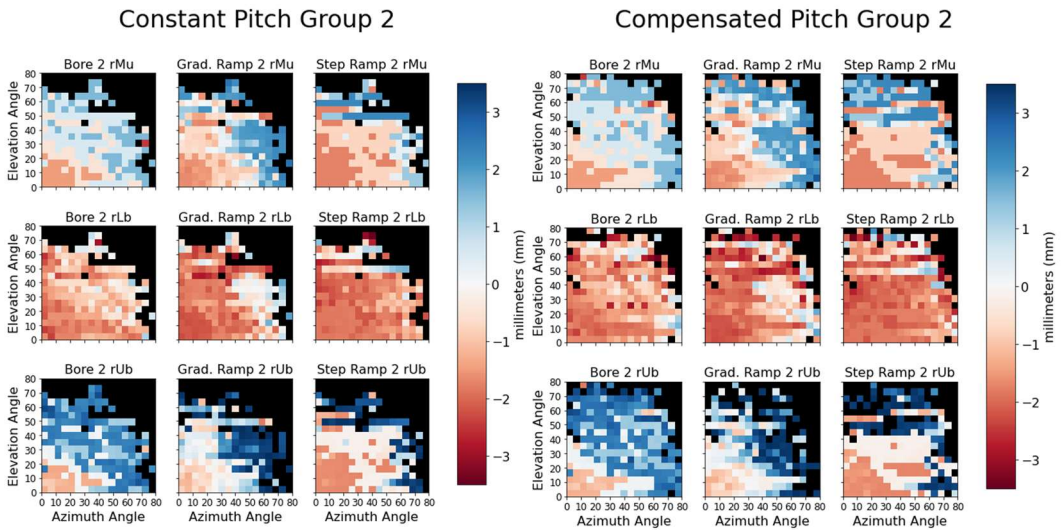


Figure 6. Residual statistics for thickness group two (absolute thickness of 6.14 – 7.42 mm, or a thickness reduction of 26% – 39%).

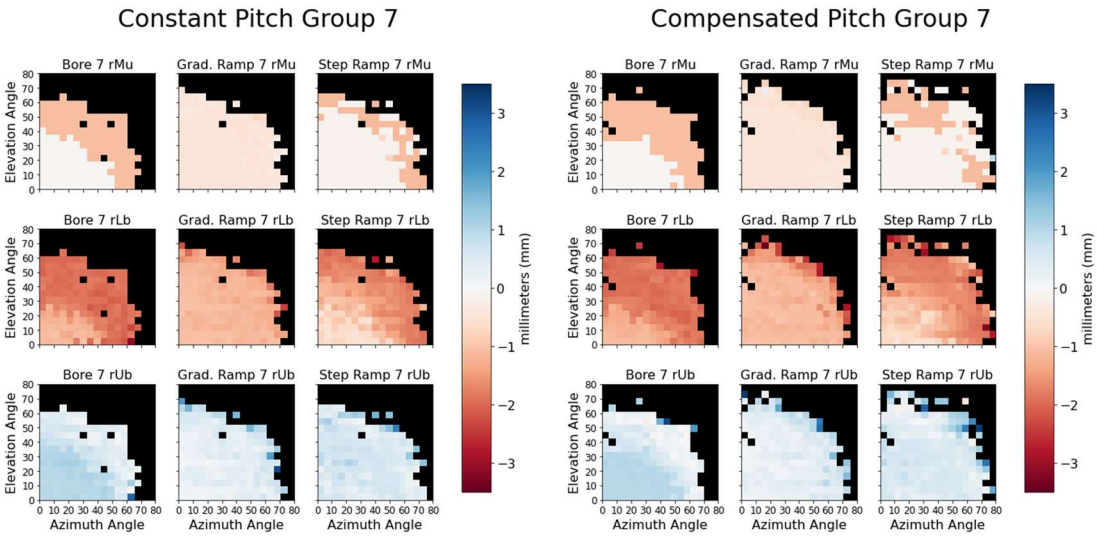


Figure 7. Residual statistics for thickness group seven (absolute thickness of 1 – 2.3 mm, or a thickness reduction of 77% – 90%).

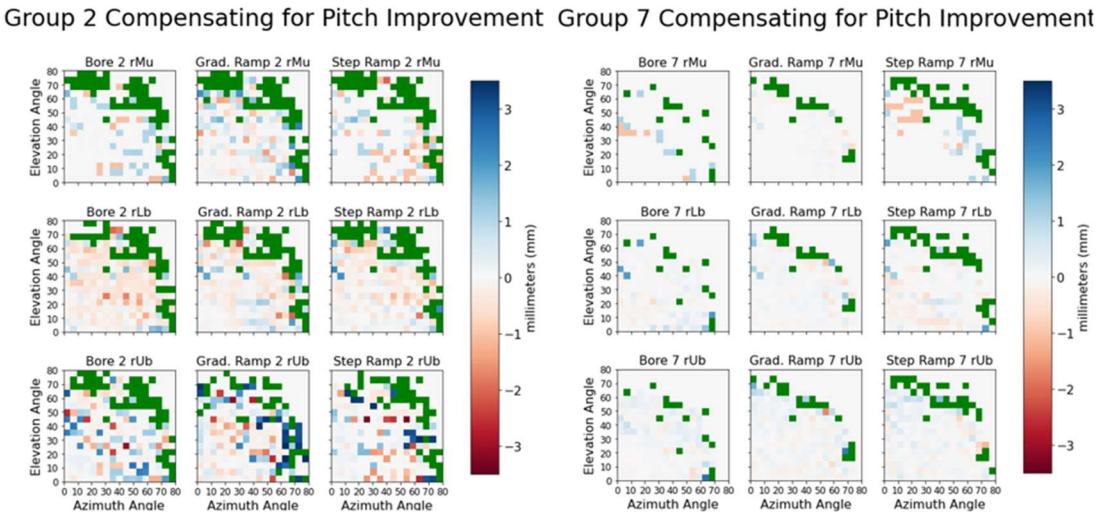

Figure 8. Improvement from compensated pitch for non-control groups, green tiles have no acceptable constant pitch scan.

Observing the medians of each residual distribution, ASSESS consistently underestimated thickness for Groups 0-6. Thus, rather than choosing traditionally well behaving residuals for the reliable operating ranges, bounds in which medians and confidence intervals behave most like 0° scans for each group are chosen. The statistics are observed to be slightly asymmetric about which direction the plate is rotated, identifying bias during the measurements. This may be because the two axes of each pixel are controlled by different hardware, or feature locations on the plate.

## CONCLUSIONS

It can be concluded that the ASSESS system has a modest ± 20° (horizontal and vertical) operating FOV for effectively estimating thicknesses greater than 5 mm (or thickness reductions less than 50%). Thicknesses less than 5 mm can be resolved up to a FOV of ± 40° (thickness reductions greater than 50%). Within the identified operating range, there is no observed improvement from compensating the measurement pitch, which rules out a hardware limitation, until the large incidence angle measurements where compensating for pitch begins improving results.

This paper demonstrates the limitations of an ultrasonic NDE method for planar specimens with non-zero incidence angles. Large thick-walled structures should be inspected from a larger stand-off distance or with multiple smaller scans, and convex structures require even tighter bounds based on the radius of curvature. Within these bounds, ASSESS can effectively resolve both gradient and discontinuous defects, and separate different characteristics if an appropriately fine constant pitch size is chosen. Increasing measurement resolution, and effectively improving the SNR, does not improve thickness estimation until an angular threshold set by the operating bounds is met, and then only enables poor estimations to be made as seen in Figure 4. Although it is prone to underestimation, uncertainty is predictable and uniform within the conservative operating bounds. The defect separation performance as seen in the ramp defect uncertainties also provides confidence in mapping out identified defects to evaluate the extent of damage in the cases of corrosion and delamination.

## FUTURE WORK

To isolate the uncertainty from the LDV's SNR alone at higher incident angles, another experiment could be performed using the method described in previous work [4]. This study could be repeated with different surface reflectivities to further characterize the hardware limits revealed directly to the amount of light reflected to the sensor. It would also be insightful to repeat this experiment with a thinner plate to evaluate ASSESS' sensitivity as result of which part of a dispersion curve is being used.

## REFERENCES


1. Michaels, Jennifer. 2017. Ultrasonic wavefield imaging: Research tool or emerging NDE method?. AIP Conference Proceedings. 1806. 020001. 10.1063/1.4974542.
2. Abbas, Muntazir, and Mahmood Shafiee. 2018. "Structural Health Monitoring (SHM) and Determination of Surface Defects in Large Metallic Structures using Ultrasonic Guided Waves" *Sensors* 18, no. 11: 3958. https://doi.org/10.3390/s18113958
3. E. B. Flynn and N. D. Stull, "Toward Utilizing Full-Field Laser-Ultrasound for Practical Nondestructive Inspection with Acoustic Wavenumber Spectroscopy," *2018 IEEE International Ultrasonics Symposium (IUS)*, Kobe, Japan, 2018, pp. 1-7, doi: 10.1109/ULTSYM.2018.8579833.
4. Fickenwirth, Peter H., Matthew J. Adams, and Eric B. Flynn. 2019. "Three-Dimensional Acoustic Wavenumber Spectroscopy for Structural Health Monitoring." Structural Health Monitoring 2019, August. doi:10.12783/shm2019/32196.
5. Cummings, Ian T., Elena C. Reinisch, Erica M. Jacobson, David H. Fraser, Adam J. Wachtor, and Eric B. Flynn. 2022. "Using Lidar to Identify Planar Measurement Regions in Ultrasonic Inspections of Complex Structures." *Proceedings of the 13th International Workshop on Structural Health Monitoring*, August. doi:10.12783/shm2021/36318.
6. E. B. Flynn and G. S. Jarmer, "High-speed, non-contact, baseline-free imaging of hidden defects using scanning laser measurements of steady-state ultrasonic vibration," presented at the Structural Health Monitoring, 2013. [Online].
7. J. Y. Jeon *et al.*, "2D-wavelet wavenumber filtering for structural damage detection using full steady-state Wavefield Laser Scanning," *NDT & E International*, vol. 116, p. 102343, 2020. doi:10.1016/j.ndteint.2020.102343
8. E. Jacobson, I. Cummings, P. Fickenwirth, E. Flynn, and A. Wachtor, "Defect detection in additively manufactured metal parts using in-situ steady-state ultrasonic response data," *Special Topics in Structural Dynamics & Experimental Techniques*, vol. 5, pp. 59–73, 2021. doi:10.1115/1.0004051v
9. Bradski, G. (2000). Th OpenCV Library. *Dr. Dobb's Journal of Software Tools*.
10. F. Pedregosa *et al.*, 'Scikit-learn: Machine Learning in Python', *Journal of Machine Learning Research*, vol. 12, pp. 2825–2830, 2011.